Biochemistry and Biophysics Reports 32 (2022) 101382

Contents lists available at ScienceDirect

Biochemistry and Biophysics Reports

journal homepage: www.elsevier.com/locate/bbrep

Treatment with hepatocyte transplantation in a novel mouse model of persistent liver failure

Yuki Tamaki [a], Yuria Shibata [a], Misaki Hayakawa [a], Nodoka Kato [a], Ami Machii [a], Yuma Ikeda [a], Eri Nanizawa [b], Yumi Hayashi [a], Hiroshi Suemizu [c], Hiroyasu Ito [d], Tetsuya Ishikawa [a,*]

[a] Department of Integrated Health Sciences, Nagoya University Graduate School of Medicine, 1-1-20 Daiko minami, Higashi-ku, Nagoya, 461-8673, Japan
[b] Department of Anatomy, Aichi Medical University, 1-1 Yazako karimata, Nagakute, Aichi, 480-1195, Japan
[c] Department of Laboratory Animal Research, Central Institute for Experimental Animals, 3-25-12 Tonomachi, Kawasaki-ku, Kawasaki, 210-0821, Japan
[d] Department of Clinical Laboratory Medicine, Fujita Health University, 1-98 Dengakugakubo, Kutsukake-cho, Toyoake, Aichi, 470-1192, Japan

ARTICLE INFO

Keywords:
Liver regeneration
Liver failure
Hepatocyte transplantation
Cellular senescence
Immune rejection

ABSTRACT

Background and Aim: Cell-based transplantation therapy using hepatocytes, hepatic stem cells, hepatocyte-like cells induced from stem cells, etc. is thought to be an attractive alternative to liver transplantation, and have been studied to date. For its clinical application, however, it is extremely important to develop a model that reproduces the pathological conditions with indication for treatment and enables the study for the ideal treatment strategy.

Methods: The transgenic mice which express the thymidine kinase (TK) gene of human herpes simplex virus (HSV) in their hepatocytes with normal immunity has been developed (designated as HSVtk). After ganciclovir (GCV) administration which injure TK-expressing hepatocytes, the primary hepatocytes (PHs) isolated from green fluorescent protein (GFP) transgenic mouse (GFP-tg) were transplanted to HSVtk intrasplenically, and replacement index (RI) with transplanted PHs in the liver, liver histology, and mRNA expressions in the liver were analyzed up to 8 weeks after transplantation.

Results: HSVtk without PH transplantation after GCV administration developed persistent liver failure with degenerated hepatocytes, persistent elevation of ALT and hepatic p16 mRNA levels, suggesting the existence of cellular senescence in the base of the disease. When autologous GFP-PHs were transplanted to HSVtk, the transplanted cells were successfully engrafted in the liver. Eight weeks after transplantation, serum ALT levels and liver histology were almost normalized, while RIs varied from 19.8 to 73.8%. Since the hepatic p16 mRNA levels were decreased significantly in these mice, the senescence of hepatocytes associated with liver injury was thought to be resolved. On the other hand, allogenic GFP-PHs transplanted to HSVtk were eliminated as early as 1 week after transplantation. In these mice, hepatic p16 mRNA levels were significantly increased at 8 weeks after transplantation, suggesting the aggravation of hepatocyte senescence. FK506 administration to HSVtk protected the transplanted hepatocytes with allogenic background from rejection at 2 weeks after transplantation, but the condition of mice and the senescent status in the liver seemed worsened.

Conclusions: The mouse model with HSVtk/GCV system was useful for studying the mechanism of liver regeneration and the immune rejection responses in the hepatocyte transplantation treatment. It may also be utilized to develop the effective remedies to avoid immune rejection.

1. Introduction

Orthotopic liver transplantation (OLT) for intractable liver diseases, such as acute and chronic liver failure and hepatocellular carcinoma, is an effective remedy proven to improve prognosis of the patients [1,2]. But there are some serious problems in conducting liver transplantation, such as lack of donors, operative damages for both recipients and donors, risk of graft rejection, and side effects of immunosuppressants [3–6]. As a substitute for OLT, treatment based on cell transplantation, such as with hepatocytes, hepatic stem cells, and hepatocyte-like cells induced from somatic stem cells or iPS cells [7–10], and organoid transplantation [11], have been studied.

For the treatment of liver failure, the strategy to use mature

* Corresponding author.
E-mail address: ishikawa@met.nagoya-u.ac.jp (T. Ishikawa).

https://doi.org/10.1016/j.bbrep.2022.101382
Received 23 August 2022; Received in revised form 3 November 2022; Accepted 4 November 2022

Abbreviations

OLT	orthotopic liver transplantation
TK	thymidine kinase
HSV	human herpes simplex virus
HSVtk	HSV-TK transgenic mouse
GCV	ganciclovir
GFP	green fluorescent protein
GFP-tg	GFP transgenic mouse
RI	replacement index
HBV	hepatitis B virus
HCV	hepatitis C virus
NOG	NOD/SCID/IL2Rg null
FK506	tacrolimus
CAG promoter	chicken beta-actin promoter and cytomegalovirus enhancer
PH	primary hepatocyte
ALT	alanine aminotransferase
Auto	autologous PH transplantation model
Allo	allogenic PH transplantation model
FK	FK506-treated *Allo* model
ASC	adipose-derived stem cell
ASC	ASC-treated *Allo* model
BW	Body weight
HE	hematoxylin and eosin
SA-β-gal	senescence-associated β-galactosidase
PCNA	proliferating cell nuclear antigen
qRT-PCR	quantitative real-time reverse-transcription PCR
ANOVA	analysis of variance test
SMA	smooth muscle actin
HGF	hepatocyte growth factor
EGF	epidermal growth factor
TGF-α	transforming growth factor-α
VEGF	vascular endothelial growth factor
EGFR	epidermal growth factor receptor
VEGFR	vascular endothelial growth factor receptor
GAPDH	glyceraldehyde 3-phosphate dehydrogenase
LSEC	liver sinusoidal endothelial cell
HSC	hepatic stellate cell
SASP	senescence-associated secretory phenotype
NFκB	nuclear factor-kappa B
Mdm2	murine double minute 2

hepatocytes for transplantation has been considered, and the clinical trials to prove its efficacy has continued for more than 2 decades [7]. Although its safety and short-term efficacy have been proven, there are unsolved issues, such as low cell engraftment rate and short-lasting effect. To solve such problems and guarantee the possibility of next-generation cell-based or organoid transplantation, the establishment of an appropriate model useful for studying an ideal methodology of cell-based transplantation therapy is extremely important.

Recently, the systems to develop human hepatocyte chimeric mice were established. The chimeric mice produced by these systems have been used mainly to reproduce hepatitis virus infection, such as hepatitis B and C virus (HBV and HCV) that infect human hepatocytes exclusively and test the effects of the antiviral drugs for these viruses. Furthermore, they have also been used to examine the metabolic efficiency of drugs and toxic substances which are known to be metabolized in human hepatocytes.

TK-NOG: severely immunodeficient NOG (NOD/SCID/IL2Rg null) mouse with targeted expression of the herpes simplex virus (HSV) type 1 thymidine kinase (TK) in the hepatocytes, has been used for developing the human hepatocyte chimeric mice. In TK-NOG mouse, the administration of ganciclovir (GCV) and subsequent transplantation of healthy human hepatocytes enables mouse liver to be stably replaced with mature and functional human hepatocytes [12,13]. Indeed, the hepatocyte chimeric mice developed from TK-NOG mice are recognized as very useful in vivo model for screening and assessment of the antiviral drugs for HBV and HCV [14]. However, at the same time, these mice have essential problem that they cannot reproduce the pathology of immunity-based liver damage, such as viral hepatitis because of their severe immunodeficiency.

In the current study, we modified TK-NOG mouse to have normal immunity in order to develop an appropriate model for hepatocyte or hepatocyte-like cell transplantation, with which the study for the mechanism of engraftment and immune rejection of the transplanted cells is possible. Namely, we backcrossed TK-NOG mice to BALB/c or C57BL/6 background, and designated these immunocompetent mice with TK expression in their hepatocytes as HSVtk mice. These HSVtk mice were transplanted with autologous or allogeneic hepatocytes after being administered with GCV. Then the mice were served for the sequential analysis of replacement rate with transplanted hepatocytes and histological and immunological changes in the liver caused by the transplantation. In addition, we examined the efficiency of immunosuppressive therapies with tacrolimus (FK506) [15–17] and adipose tissue-derived mesenchymal stem cells (ASCs) [18,19] to avoid immune rejection of the transplanted cells.

2. Materials and methods

2.1. Animals

HSVtk mice expressing TK in the liver under the control of an albumin promoter, backcrossed onto inbred C57BL/6 or Balb/c and acquired normal immune system, were obtained from Central Institute for Experimental Animals (CIEA, Kawasaki, Japan). Backcrossing to the individual strains of mice was continued 9 to 10 times in our facility to establish HSVtk with complete inbred background of C57BL/6 (H-2^b) and BALB/c (H-2^d), and these mice were designated as HSVtk/BL6 and HSVtk/Balb, respectively (Fig. 1a, Suppl. Table 1). Green fluorescent protein (GFP)-transgenic mice with C57BL/6 background (GFP-tg, H-2^b) which systemically express GFP under the control of a chicken beta-actin promoter and cytomegalovirus enhancer (CAG promoter), were purchased from RIKEN Bio Resource Research Center (Kanagawa, Japan). C57BL/6 and BALB/c mice were purchased from Chubu Kagaku Shizai Co., Ltd. (Aichi, Japan). All the mice were housed in a controlled environment (12 h light/dark cycles at 25 °C) with free access to water and chow (CE2; CLEA Japan, Tokyo, Japan; DietGel Recovery, Clear H_2O, Portland, ME). All conditions and handing of animals in this study were conducted in accordance with the National Institutes of Health guide for the care and use of Laboratory animals (NIH Publications No. 8023, revised 1978), and under the protocols approved by Nagoya University Committee on Animal Use and Care (#031–35, #20042, #D210671, #D220046). The numbers of mice used in the individual experiments are described in the figure legends.

2.2. Primary hepatocyte (PH) isolation

PHs were isolated from 6 to 11 weeks old GFP-tg. In brief, mice were anesthetized with isoflurane (Pfizer Inc., New York, NY), and the liver was rinsed with 20 ml prewarmed (47 °C) Liver Perfusion Medium (17703-038; Gibco) through the abdominal inferior vena cava. Then, the liver was perfused with Liver Digest Medium (17703-034; Gibco) containing Liberase™-TM (5401127001; Roche). The digested liver was aseptically transferred to sterile tube containing 20 ml cold PBS. Isolated

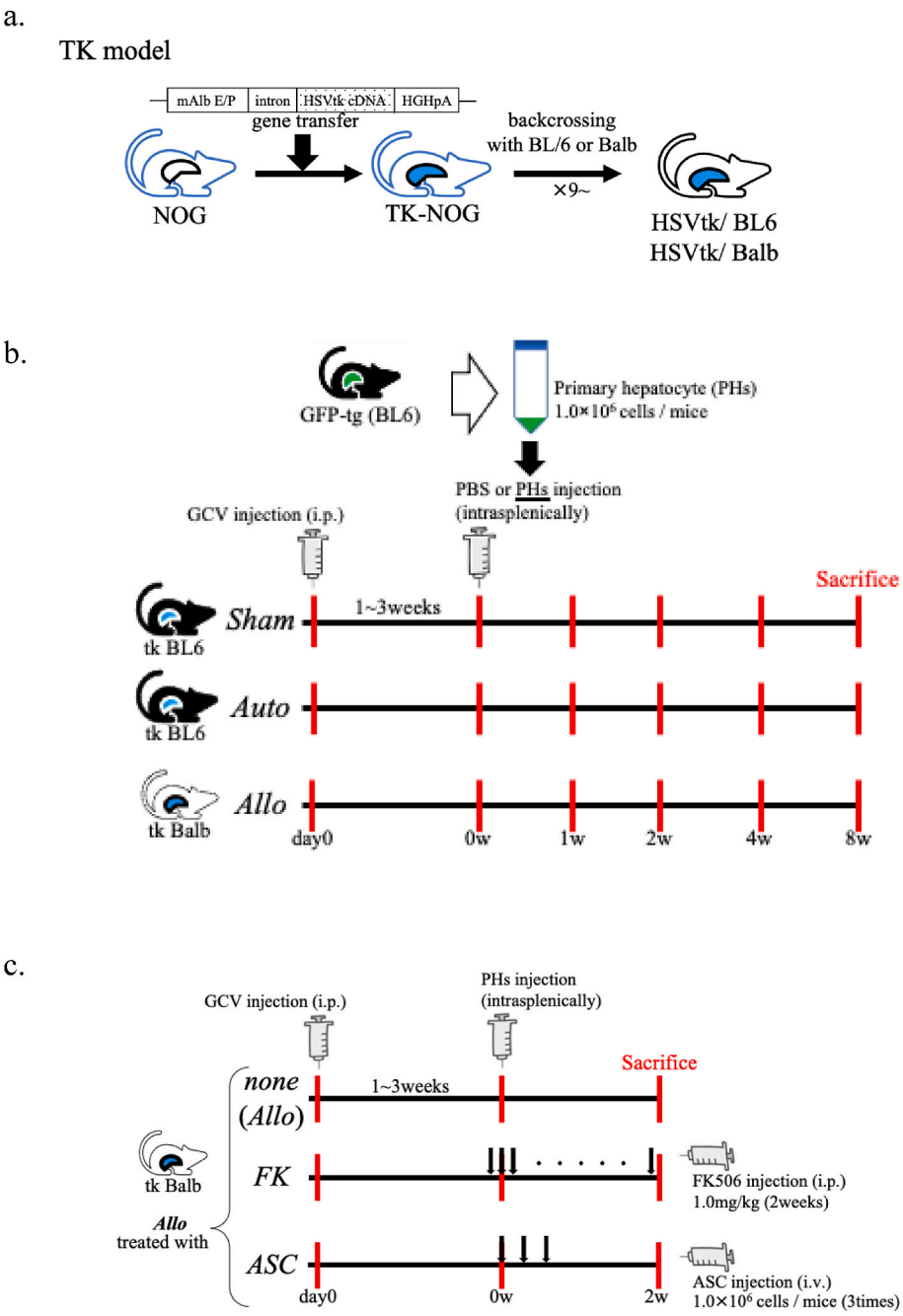

Fig. 1. Experimental scheme.
a. The construction of HSVtk model. TK-NOG mouse is a transgenic mouse with NOG background, in which the mouse albumin enhancer/promoter (mAlb E/P), the chimeric intron, HSVtk cDNA, and the 3′-UTR of the human growth hormone gene with a polyadenylation signal (hGH pA) are integrated in its genome, and expresses HSV-TK only in the liver. We established an immunocompetent mice by backcrossing TK-NOG mice to C57BL/6 or BALB/c mice 9–10 times or more (designated as HSVtk/BL6 and HSVtk/Balb).
b. Method of hepatocytes transplantation. GCV was intraperitoneally injected to HSVtk/BL6 or HSVtk/Balb, and primary hepatocytes (PHs) isolated from GFP-tg were transplanted after the ALT level reached 500 U/L (*Auto* or *Allo* model). HSVtk/BL6 administered with PBS after administered of GCV was used a control (*Sham*).
c. Treatment model for immune rejection against allogenic hepatocytes. HSVtk/Balb after GCV administration was transplanted with PHs isolated from GFP-tg with BL/6 background (*Allo* model). FK506 was intraperitoneally administered every day from the day before transplantation until the day of sacrifice (*FK* model). ASCs were intravenously administered three times on the day of transplantation, 3 days and 6 days after transplantation (*ASC* model). *Allo* model without treatment was used as control. All the mice were sacrificed for analyses two weeks after transplantation.

hepatocytes were dispersed into single cell suspension with a large bore pipette, and passed through a sterile 40 μm nylon mesh (Thermo Fisher Scientific Inc.) into a new sterile tube. The cell suspension passed through the mesh was centrifuged at 50×*g* at 4 °C for 3 min, and the resulting cell pellet was resuspended in cold PBS. Then the cells were counted, and viability of the cells were assessed using the trypan blue exclusion test.

2.3. GCV administration and PH transplantation

GCV (Mitsubishi Tanabe Pharma Corp., Osaka, Japan) was intraperitoneally administered to 7–10 weeks old HSVtk mice. For enabling engraftment of transplanted hepatocytes in the liver and avoiding loss of mice, it is necessary to adjust the ALT levels after GCV administration to 500–2000 U/L. Since HSVtk/Balb is more susceptible to GCV than HSVtk/BL6, the dose of GCV was adjusted to 50 μg/g (mouse weight) for HSVtk/Balb and 100 μg/g for HSVtk/BL6. One week after GCV administration, blood samples were subjected to the analysis of alanine aminotransferase (ALT) levels. ALT measurement was performed using transaminase CII-Test kit (Wako) or entrusted to SRL Inc. (Aichi, Japan). Transplantation was carried out when ALT level reached 500 U/L or higher. In case ALT level was lower than 500 U/L, additional GCV administration was executed. One week after the last GCV administration, GCV-treated mice were transplanted with 1 x 10^6 of PHs (in 400 μl PBS) from GFP-tg mice intrasplenically. HSVtk/BL6 and HSVtk/Balb transplanted with GFP-tg-derived PHs were defined as autologous PH transplantation (*Auto*) and allogenic PH transplantation model (*Allo*), respectively. HSVtk/BL6 without cell transplantation but injected with 400 μl PBS alone was designated as *Sham* model (Fig. 1b, Suppl. Table 1).

2.4. Treatment with tacrolimus against immune rejection of transplanted PHs

FK506 stock (Astellas Pharmaceutical, Inc., Tokyo, Japan) was dissolved in PBS and adjusted to a working concentration of 0.08 mg/mL. For the treatment against immune rejection in *Allo* model, the mice were administered with 1.0 mg/kg FK506 intraperitoneally every day from one day before transplantation [16,17]. This model was designated as *FK* model (FK506-treated *Allo* model, Fig. 1c, Suppl. Table 1).

2.5. Preparation of adipose-derived stem cells (ASCs) and treatment against immune rejection with ASCs

ASCs were isolated as previously reported elsewhere with minor modification [18,19]. Inguinal subcutaneous adipose tissues were taken from 6 to 7 weeks old female BALB/c mice, the tissues were placed in Dulbecco's modified Eagle Medium Nutrient Mixture F-12 (DMEM, Life Technologies Corporation, NY, USA) containing 20% fetal bovine serum (FBS; Life Technologies), and minced finely adding 500 μl of Hanks' balanced salt solution (HBSS; Life Technologies). The pooled, minced tissues were incubated in 10 ml of HBSS containing collagenase Type I (Funakoshi Co Ltd, Tokyo, Japan) at 37 °C for 60 min. The suspensions of these tissues were passed through a sterile 100 μm mesh, and resuspended in DMEM. After centrifugation at 1200 rpm for 10 min, the isolated cells were washed with DMEM and resuspended in DMEM containing 20%FBS. Then, the cells were seeded on 75 cm^2 flasks (Thermo Fisher Scientific Inc), the attached cells were cultured as the progenitors of ASCs. After 4 to 6 passages, thus cultured ASCs were used for the treatment against immune rejection of transplanted PHs. Namely, ASCs were collected, and 1 x 10^6 cells were resuspended in 190μl PBS with 10 μl Novo-Heparin (1,000 Units/mL, Mochida Pharmaceutical, Tokyo, Japan), and administered via the tail vein on the day of PH transplantation and 3, 6 days after transplantation in *Allo* model [20]. This model was designated as *ASC* model (ASC-treated *Allo* model, Fig. 1c, Suppl. Table 1).

2.6. Body weight measurement and sample collection after transplantation

Body weight (BW) measurement and blood sample collection were performed at the time of GCV administration, and weekly after PH transplantation. Sera were stored at - 20 °C until use, and they were subjected to the measurement of serum ALT levels (SRL Inc. Aichi, Japan). In all the models (*Sham, Auto*, *Allo, FK*, and *ASC* models), the mice were sacrificed at before (day 0) and 1 week after GCV administration (0 w), 1, 2, 4, and 8–11 weeks after PH transplantation (1, 2, 4, and 8 w, respectively). The resected livers were subjected to the histological analysis, flow cytometric analysis for hepatocyte polyploidy, and hepatic gene expression analysis (Fig. 1b and c). The part of liver tissues was fixed with 10 N Mildfolm (Wako) at room temperature for the histological examination. The unfixed liver tissues were embedded with FSC 22 Clear Frozen Section Compound (Leica Biosystems, Germany), and frozen in liquid nitrogen for the preparation of frozen specimens also for another histological examination. The remaining part of them were stored at -30 °C in RNAlater (QIAGEN, Hilden, Germany) for the analysis of mRNA expression. For the flow cytometric analysis, the livers were perfused as described above (2.2 PH isolation) to collect isolated hepatocytes.

2.7. Histological analysis

The fixed liver tissue was embedded with paraffin and sliced to a thickness of 4 μm by using a microtome. Staining with hematoxylin & eosin (HE), Azan, and immunostaining for GFP and Proliferating Cell Nuclear Antigen (PCNA) was performed using tissue specimens. The unfixed liver tissue was sliced to thickness of 8 μm by using a cryostat, and stained with senescence-associated β-galactosidase (SA-β-gal).

GFP and PCNA-immunostaining was performed according to the Cell Signaling Technology's protocol for immunochemical staining (paraffin). GFP (D5.1) XP® Rabbit mAb (Cell Signaling Technology, Danvers, MA) was diluted 200 times, and PCNA (D3H8P) XP® Rabbit mAb (CST) 4000 times for use. The Senescence β-Galactosidase Staining Kit (CST) was used according to manufacturer's instructions for β-gal staining.

The liver specimens were microscopically observed and photographed by DP 73 (analyzed by Cell sense, Olympus, Tokyo, Japan), and the overall images of the livers with immunostaining was taken with BZ-9000 (Keyence, Osaka, Japan). The percentages of GFP immunostaining-positive part (replacement index: RI) and the area of Azan staining-positive region were quantified using ImageJ (Wayne Rasband, NIH, USA). The images of HE- and PCNA-stained specimens were examined using BZ-X800 (Keyence) and BZ-X800 Analyzer software for the measurement of nucleus sizes and PCNA positive ratios.

2.8. Flow cytometry for DNA polyploidy analysis

Cell Cycle Phase Determination Kit (Cayman chemical company) was used to analyze cell cycle alterations and DNA polyploidy in PHs isolated from the *Allo* model at 8 w. The collected PHs were passed through a sterile 40 μm nylon mesh, and washed twice with cold PBS and assay buffer, respectively. After the centrifugation, the cell pellet was resuspended to density of 1 x 10^6 cells/ml in assay buffer, and added an equal volume of cell cycle phase determination fixative to each sample to fix and permeabilize the cells and place at -20 °C for at least 2 h. The fixed cells were centrifuged at 500 G for 5 min, and resuspended in 0.5 ml staining solution. After incubating for 30 min at room temperature in the dark, the samples were analyzed using FACS Canto2 (BD Biosciences).

2.9. Quantitative real-time reverse-transcription PCR (qRT-PCR) analysis

Quantitative real-time reverse-transcription polymerase chain reaction (qRT-PCR) was performed using total RNA prepared from liver tissue with NucleoSpin® RNA (Takara Bio Inc., Shiga, Japan). The RNA was subjected for first-strand cDNA synthesis using PrimeScript RT Master Mix (Takara Bio Inc.) according to the manufacturer's instructions. qRT-PCR was performed with Thermal Cycler Dice Real Time System II (Takara Bio Inc.) using TB Green™ Premix Ex Taq™ II (Tli RNaseH Plus, Takara Bio Inc.) according to the manufacturer's instructions. The PCR amplification was performed as follows; an initial denaturing step, at 95 °C for 30 s; followed by 40 cycles, at 95 °C for 5 s; at 60 °C for 30 s. Measured items and their primers in this experiment are listed in Suppl. Table 2.

2.10. Statistical analyses

All the values were expressed as the mean ± SD (standard deviations). Data were analyzed by two-way analysis of variance test (ANOVA) followed by Steel-Dwass tests for multiple group comparison. All analyses were performed with EZR (Saitama Medical Center, Jichi Medical University, Saitama, Japan) [21], which is a graphical user interface for R (The R Foundation for Statistical Computing, Vienna, Austria). A significant difference was defined as a p-value of <0.05.

3. Results

3.1. Sequential changes of BW and ALT levels

First, we evaluated sequential changes of BW and serum ALT levels in *Sham*, *Auto*, and *Allo* models. BW ratios (the ratios of BW at the individual time point to BW just before PH transplantation) and serum ALT levels were weekly measured from 0 to 8 w. There were no significant changes in BW ratios and ALT levels among three models until 4 w.

However, BW ratios were significantly higher and ALT levels were significantly lower in the *Auto* model compared with the *Sham* and *Allo* models at 8 w. ($p < 0.05$, respectively, Fig. 2a and b, Suppl. Table 3a, b). These indicate that the nutritional status and liver injury were ameliorated only in the *Auto* model.

3.2. Replacement indices (RIs) by transplanted hepatocytes

In the *Auto* model, GFP immunostaining indicated that average RIs by the transplanted GFP-expressing hepatocyte at 1, 2, 4, and 8 w were $1.2 \pm 1.5\%$, $11.5 \pm 13.2\%$, $28.1 \pm 6.1\%$ and $46.2 \pm 23.2\%$, respectively (Fig. 3b). RIs of 8 w varied from 19.8 to 73.8%. Representative image of the whole liver immuno-stained with GFP (that of HSVtk at 8 w showing RI of 54.7%) is presented in Suppl. Fig. 1a, and those of the GFP-stained liver sections at the individual time points are presented in Fig. 3a. These indicate that the transplanted, engrafted hepatocytes gradually proliferated at least up to 8 w in the *Auto* model. On the other hand, in the *Allo* model, the GFP-positive hepatocytes were not detected both in the histological and qRT-PCR analysis already at 1 w (Fig. 3b and c), indicating that the transplanted PHs were eliminated before one week after the transplantation or earlier.

3.3. Changes of liver histology

The histological images of HE staining in each model are shown in Fig. 4a. In all the models at 0 w, many of the hepatocytes were degenerated with enlarged eosinophilic cytoplasms, and sporadic infiltration of inflammatory cells were observed mainly in the lobules. Apoptosis-like cells scattered in the lobules were observed at 0 w. In the *Sham* and *Allo* models, the extent of hepatocyte degeneration worsened over time, and most of the hepatocytes were degenerated at 8 w. Furthermore, inflammatory cell infiltration was continuously observed up to 8 w, but apoptotic cells and necrotic foci were rarely observed in both models. In the *Auto* model, inflammatory cell infiltration tended to be pronounced compared with in the *Sham* and *Allo* models at 2 w, but it decreased at 4 w and almost disappeared at 8 w. The extent of degeneration in the hepatocytes were reduced at 4 w, and most of the hepatocytes exhibited a nearly normal morphology at 8 w.

In Azan staining, no apparent fibrosis was observed at any time point in the *Auto* model. On the other hand, slight fibrosis around hepatocytes was observed in the *Sham* model at 8 w, and they were more evident in the *Allo* model at 8 w. The areas of Azan staining-positive regions quantified by the image analysis were significantly increased at 4 and 8 w compared with those at 2 w or earlier in the *Sham* and *Allo* models, and the increase was more evident in the *Allo* model than in the *Sham* model. Azan staining-positive regions was not observed in the *Auto* model. (Fig. 4b).

Interestingly, there were clusters of small hepatocytes resembling regenerating nodules adjacent to the portal region only in the *Sham* and *Allo* models at 8 w (Suppl. Fig. 1b). It is possible that these small hepatocytes forming the nodules were differentiated from the hepatic stem cells in the canals of Hering, and it suggests that current model well reproduced the features of severe persistent liver failure.

3.4. Changes of the sizes of the hepatocyte nuclei

We evaluated the proliferation efficiency of the hepatocytes by examining the percentages of PCNA-positive nuclei during the observation period in all the models. The rates of PCNA-positive nuclei at 8 w showed no apparent changes among the individual models (Fig. 4c). Since the enlargement of nuclei was histologically observed in the *Sham* and *Allo* models, the sizes of hepatocyte nuclei were quantized during the observation period to determine whether the percentage of PCNA-positive nuclei truly reflected the degree of cell proliferation.

The sizes of nuclei were evaluated using images of HE staining. In the *Auto* model they were slightly larger after transplantation compared with those before transplantation, but the changes were not prominent. In contrast, the sizes of nuclei in the *Sham* and *Allo* models increased over time during the observation period, and this tendency was more prominent in the *Allo* model. When nuclear sizes were plotted as histograms, their variance was greater in the *Sham* and *Allo* models compared with the *Auto* model. (Suppl. Fig. 2).

We performed quantitative analysis of DNA in cell nuclei by flow cytometry to confirm if the enlargement of nuclei was associated with polyploidy, but no polyploidy was observed in the hepatocytes in the *Allo* model at 8 w (data not shown). Therefore, the enlargement of the nuclei was thought to be related to impairment of DNA replication and subsequent impairment of nucleus/cell division.

3.5. The hepatic mRNA expression of cytokines/chemokines and cell surface markers

To elucidate the mechanism of liver regeneration and immune rejection against transplanted hepatocytes, we investigated hepatic mRNA expression related to inflammatory responses.

First, we analyzed the sequential changes of mRNA expressions of inflammatory cytokines. In the *Sham* model, the mRNA levels of TNF-α (*Tnfa*) and TGF-β (*Tgfβ*) remained high until 8 w compared with those at day 0. The mRNA levels of IL-1β (*Il1b*), IL-6 (*Il6*) and IL-10 (*Il10*) also showed same tendency while they tended to decline at 8 w.

In the *Auto* model, the mRNA levels of TNF-α, IL-1β, IL-10, and TGF-β peaked at 1 to 2 w, declined thereafter, and fell to the levels equivalent to those of day 0 by 8 w. The mRNA levels of IL-6 also showed similar tendency. Notably, TNF-α and TGF-β mRNA levels at 2 w were

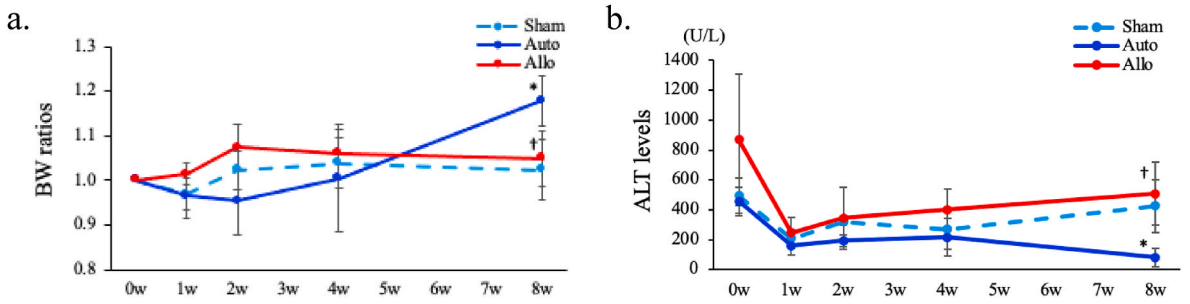

Fig. 2. Changes of BW and ALT levels.

a. Sequential changes of BW ratios in *Sham*, *Auto*, *Allo* models. The BW ratio (the ratio of BW at each time point to BW just before PH transplantation) was calculated for each week until 8 weeks after PH transplantation. 0 w means the time point before PH transplantation. All the data are expressed as mean ± SD. *$p < 0.05$ (*Auto* vs *Sham* on same week), †$p < 0.05$ (*Allo* vs *Auto* on same week). $n = 3$ in each group.

b. Sequential changes of ALT levels in *Sham*, *Auto*, *Allo* models. ALT levels were measured every week from 0 to 8 weeks after PH transplantation. All the data are expressed as mean ± SD. *$p < 0.05$ (*Auto* vs *Sham* on same week), †$p < 0.05$ (*Allo* vs *Auto* on same week). $n = 3$ in each group.

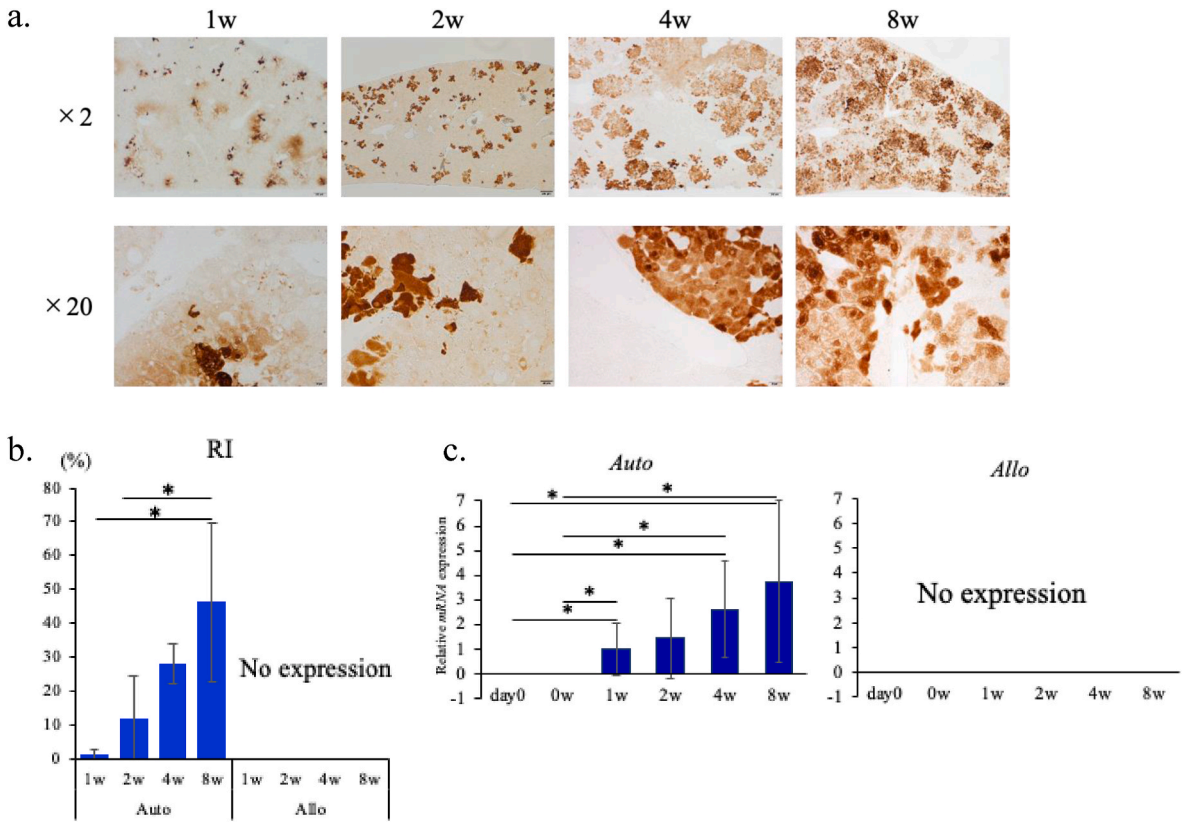

Fig. 3. Engraftment of transplanted PHs.

a. GFP-immunostaining in the liver of *Auto* model. Representative histological images of GFP-immunostained liver sections from the mice sacrificed at each time point (time after PH transplantation) are presented. From left to right, the liver images of the mice 1, 2, 4, 8 weeks after transplantation, respectively. 2 × objective's scale bar: 200 μm, 20 × objective's scale bar: 20 μm

b. Average values (%) of hepatocyte replacement indecies (RIs). GFP-positive areas of the tissue samples were calculated using ImageJ. All the data are expressed as mean ± SD. *$p < 0.05$. n = 3 in each group.

c. Hepatic GFP mRNA expression in *Auto* and *Allo* models. Hepatic mRNA expression levels were measured by qRT-PCR. Expression levels of the respective mRNAs were normalized to that of GAPDH and the data were presented as fold change compared with the average of *Auto* model at 1 week after PH transplantation. All the data are expressed as mean ± SD. *$p < 0.05$ n = 3 in each group.

significantly higher in the *Auto* model than in the *Sham* model ($p < 0.05$).

In the *Allo* model, the mRNA levels of all the cytokines increased at 0 w and remained elevated until 8 w. Particularly, the mRNA levels of TNF-α, IL-1β, and IL-6 tended to increase at 8w (Fig. 6a).

Next, we analyzed mRNA expression of the cell surface makers of inflammatory cells. In the *Auto* model, the mRNA levels of CD3 (*Cd3*), CD8a (*Cd8a*), CD11b (*Cd11b*), CD11c (*Cd11c*), and NKp46 (*Nkp46*) peaked at 1 to 2 w, declined thereafter, and tented to fall to the levels at 0 w or lower by 8 w. The mRNA levels of CD8a, CD11b, CD11c in the *Auto* model were significantly higher than those in the *Sham* model at 1 or 2 w ($p < 0.05$), while the mRNA levels of CD11b and CD11c in the *Auto* model became lower than those in the *Sham* model at 8 w ($p < 0.05$). In the *Sham* and *Allo* model, the changing patterns in the mRNA levels of CD3, CD8a, CD11b, CD11c, and NKp46 showed same tendency, namely they were increased at 0 w and maintained higher levels compared to day 0 levels until 8 w (Fig. 5b). There were no apparent differences in the kinetics of CD4 mRNA (*Cd4*) levels among all the models, all showing gradual decrease from 1 to 8 w. The mRNA levels of CD19 (*Cd19*) did not show significant changes during observation period in all the groups of mice (data not shown).

We also examined the sequential changes of hepatic mRNA levels of chemokines. Most of the chemokines showed the similar tendency to those of cell surface markers within the individual groups (Suppl. Fig. 3a). The mRNA kinetics of cell surface markers and cytokines/chemokines seem to correspond to the histological findings of the individual groups (Fig. 4a).

3.6. The hepatic mRNA expression of growth factors and cell cycle-related molecules

Since the histology suggested impaired liver regeneration in the *Sham* and *Allo* models, we examined the mRNA expression levels of growth factors and cell cycle-related markers.

The mRNA levels of HGF (*Hgf*) in the *Sham* and *Auto* models elevated during 0–2 w compared with the day 0 levels, and tended to decline thereafter. But HGF mRNA levels in the *Sham* model at 8 w tended to be elevated and was significantly higher than those in the *Auto* model. HGF mRNA levels in the *Allo* model were tended to be elevated throughout the observation period compared with levels at day 0 (Fig. 5c). EGF (*Egf*), TGF-α (*Tgfa*), and VEGF (*Vegf*) mRNA levels were elevated compared with the day 0 levels in all the models from 0 to 8 w. In the *Auto* and *Allo* models, VEGF mRNA levels were highest at 8 w during the observation period (Suppl. Fig. 3b).

HGF is known to be the most potent growth factor for hepatocytes, and its production is stimulated by inflammatory cytokines, such as IL-1, TNF-α, and IL-6. It is also known to be produced in hepatic stellate cells (HSCs) and liver sinusoidal endothelial cells (LSECs) [22]. The reason why the increase in HGF in the *Allo* model was not as high as in the *Sham* and *Auto* models is unknown, but it may be related to the influence on LSECs or HSCs by the rejection responses of the transplanted PHs.

The mRNA levels of p16 (*P16*) and p21 (*P21*) which are related to the

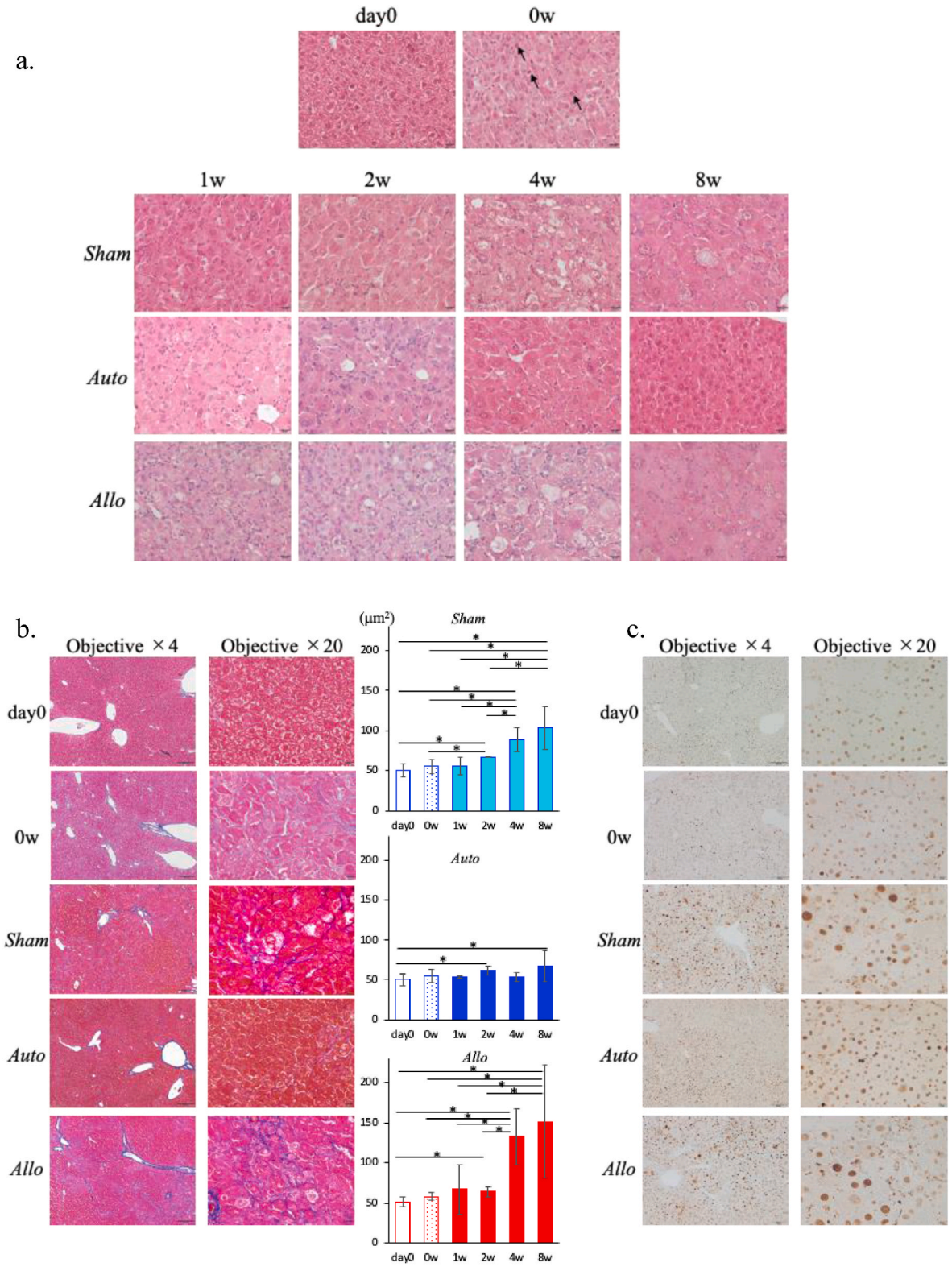

Fig. 4. Liver histology.

a. Histological analysis with H&E staining at day 0, 0 w (upper row) and each time point after PH transplantation in *Sham* (second row), *Auto* (third row), and *Allo* (lower row) models. Arrowheads (↑) indicate the apoptosis-like cells. Magnification of objective × 20 (scale bar: 20 μm)

b. Histological analysis stained with Azan at day 0 (upper row), 0 w(second row) and 8 weeks after transplantation in *Sham* (third row), *Auto* (fourth row), and *Allo* (lower row) models. 4 × objective's scale bar: 200 μm, 20 × objective's scale bar: 20 μm. The graph shows the Azan-positive area measured by the Image J software. *$p < 0.05$. $n = 3$ in each group.

c. Histological analysis stained with PCNA at day 0 (upper row), 0 w(second row) and 8 weeks after transplantation in *Sham* (third row), *Auto* (fourth row), and *Allo* (lower row) models. 4 × objective's scale bar: 200 μm, 20 × objective's scale bar: 20 μm.

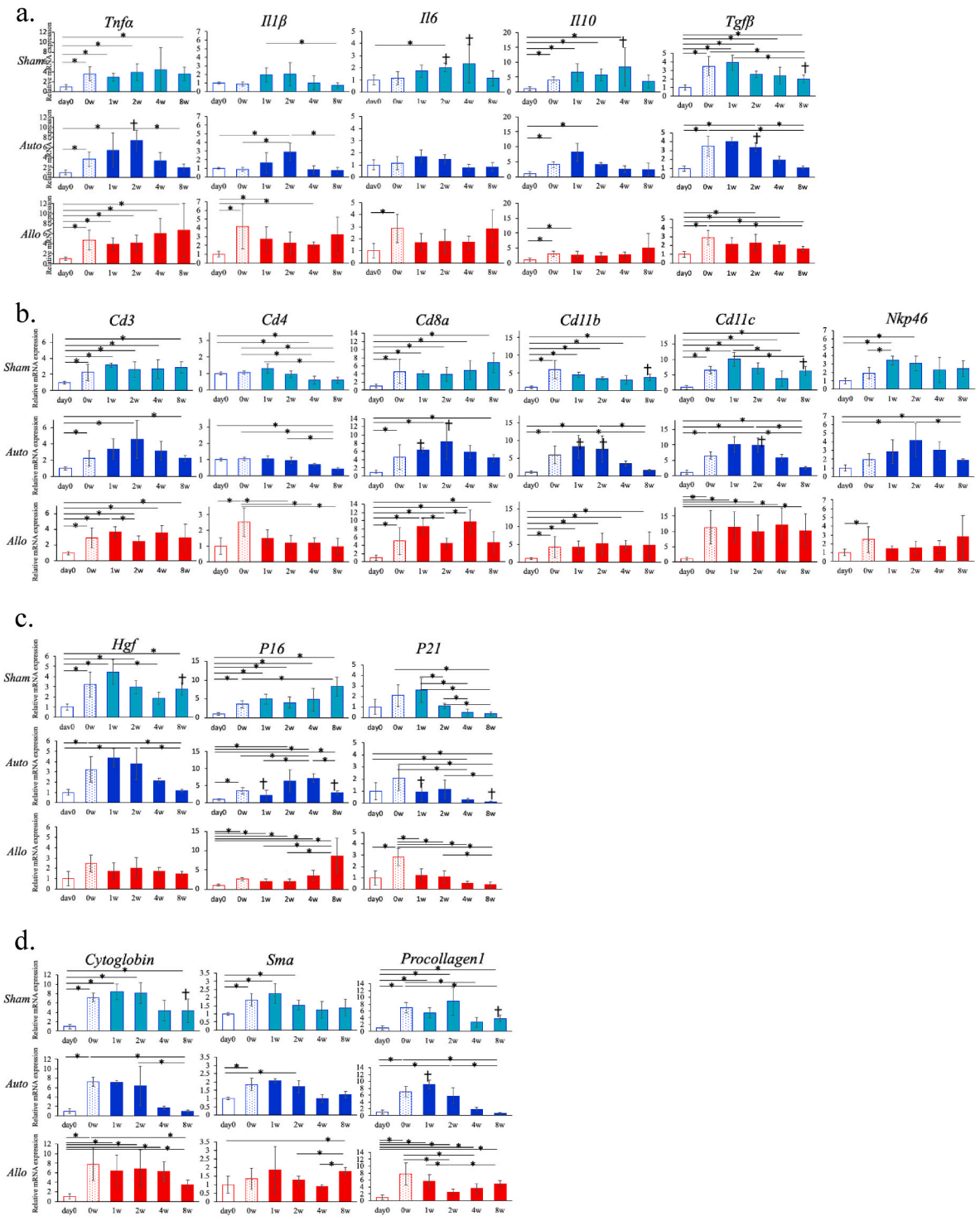

Fig. 5. Hepatic mRNA expressions.

Intrahepatic mRNA expression levels were measured by qRT-PCR. Expression levels of the respective mRNAs were normalized to that of GAPDH. The normalized data were presented as fold change compared with HSVtk/BL6 at day 0 for *Sham* and *Auto* models, and HSVtk/Balb at day 0 for *Allo* model (*$p < 0.05$, $^{\dagger}p < 0.05$ in comparison of the values between *Sham* and *Auto* models at the same time point). All the items were listed in the order of upper graph, that of *Sham*, *Auto* and *Allo* model. All the data are expressed as mean ± SD. n = 3–5 in each group.

a-c. The mRNA expression of inflammatory cytokines(a), cell surface lineage makers (b), growth factors (c), fibrosis makers (d).

cell-cycle regulation and also known as markers of cellular senescence, were evaluated.

In the *Sham* model, the mRNA levels of both p16 and p21 were increased at 0 w compared with those of day 0 levels. The mRNA levels of p16 remained high up to 4 w, and further increased at 8 w. On the other hand, the mRNA levels of p21 declined from 2 w, and became lower than those of day 0 after 4w.

In the *Auto* model, the mRNA levels of p16 increased at 0 w, temporally decreased at 1w, increased again to the higher levels at 2, 4 w, and decreased to the 2 w levels at 8 w. The mRNA levels of p21 increased at 0 w, decreased at 1 and 2 w, and further decreased at 4 and 8 w below the levels at day 0.

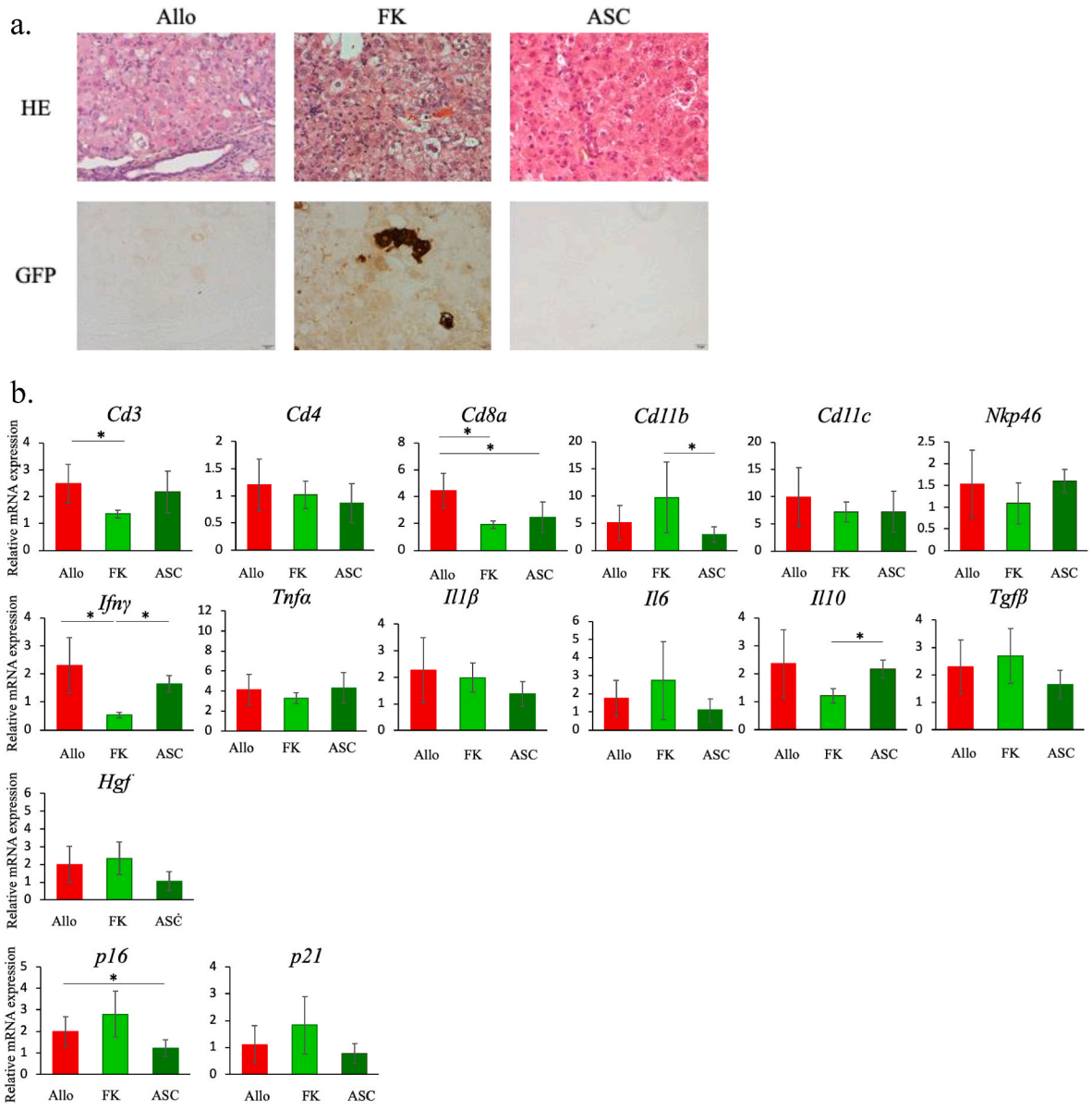

Fig. 6. The effect of the treatment against immune rejection.

a. Liver histology in treatment models against immune rejection. H&E (upper row) and GFP immunostaining (lower row) of representative liver sections from each group of mice. From left to right, *Allo*, *FK*, and *ASC* models, respectively. Magnification of objective × 20 (scale bar: 20 μm)

b. Hepatic mRNA expressions in the treatment models. Hepatic mRNA expression levels were measured by qRT-PCR. Expression levels of the respective mRNAs were normalized to that of GAPDH, and presented as fold change compared with HSVtk/Balb day 0 for *Allo* model. All the data are expressed as mean ± SD. *$p < 0.05$. n = 3–5 in each group.

The mRNA levels of p16 and p21 at 1 and 8 w in the *Auto* model were significantly lower than those in the *Sham* model ($p < 0.05$).

In the *Allo* model, the kinetics of p16 and p21 mRNA levels were similar to those of the *Sham* model. However, p16 and p21 mRNA levels at 1 and 2 w were significantly lower than those in the model without PH transplantation ($p < 0.05$).

While p16 and p21 are used as cellular senescence markers, p16 is considered to be a more favorable cellular senescence marker [23]. Although the β-gal staining of the liver specimen did not efficiently identify positive cells (data not shown), elevated p16 mRNA levels at 4 to 8 w in the *Sham* and *Allo* models were thought to associate with the senescence of hepatocytes in these models. And it appears to be consistent with the findings of histological features and impaired DNA replication in hepatocytes in these models.

The mRNA levels of Cyclin D (*Cyclin d*) and Cyclin E (*Cyclin e*) in all the models were also elevated compared with those of day 0 levels, while those in the *Auto* model tended to decline at 8 w (Suppl. Fig. 3b). These also suggests the existence of cell cycle arrest in G1/G2 phase in these models.

3.7. The hepatic mRNA expression of fibrosis markers

Liver fibrosis usually develops as a result of persistent inflammation in the liver. Without alleviation of inflammation, liver fibrosis eventually progresses and results in the development to liver cirrhosis. Since we observed fibrosis around hepatocytes in the *Sham* and *Allo* model at 4 to 8 w, we measured the mRNA levels of early profibrotic biomarker genes, procollagen type 1 (*Procollagen1*) and α-SMA (α-smooth muscle actin, *Sma*) to analyze the mechanism of liver fibrosis development, and Cytoglobin (*Cytoglobin*) mRNA levels as a biomarker of HSC activation.

In the *Auto* model, mRNA levels of all the markers increased until 2 w, but decreased thereafter to the level close to those of day 0. In the *Sham* and *Allo* models, mRNA levels of all the markers were increased compared to day 0 levels during the observation period, and it seems compatible to the emergence of fibrosis in the liver in these models (Fig. 5d).

Since we could not find apparent difference in mRNA levels of fibrosis markers between the *Sham* and *Allo* model, the reason why the extent of fibrosis was more severe in the *Allo* model than in the *Sham* model, could not be well explained.

3.8. Therapeutic effect of FK506 or ASCs against immune rejection of transplanted hepatocytes

Using the *Allo* model as an immune rejection model against transplanted hepatocytes, we tested the efficacy of FK506, potent inhibitor of T cell activation, and ASCs which show immunosuppressive effect on various inflammatory cells (Fig. 1c).

BW ratio of the *FK* model decreased compared with that of the *Allo* model at 2 w. ALT levels were not different between the *FK* and *Allo* model. On the other hand, in the *ASC* model, ALT levels mildly declined compared with those in the *Allo* model at 1 w, and the decrease of BW ratio was tended to be suppressed compared with the *Allo* model (Suppl. Fig. 4a and b).

In the *FK* model, engraftment of GFP-positive hepatocytes was confirmed both in histology with GFP immunostaining and hepatic expression of GFP mRNA. However, HE staining showed degeneration of many of the hepatocytes and considerable inflammatory cell infiltration in the *FK* model as seen in the *Allo* model. In the *ASC* model, engraftment of GFP-positive hepatocytes was not observed, but the extent of hepatocyte degeneration and inflammatory cell infiltration seemed milder than in the *Allo* and *FK* models (Fig. 6a, Suppl. Fig. 4d).

In order to analyze the mechanism of action of the treatment, we examined hepatic mRNA expression of cytokines, cell surface markers, etc. In the *FK* model, IFN-γ mRNA levels were significantly lower compared with those in the *Allo* and *ASC* models ($p < 0.05$), and CD3 and CD8a mRNA levels were significantly lower compared with those in the *Allo* model ($p < 0.05$). In the *ASC* model, IL-10 mRNA levels were significantly higher and CD11b significantly lower compared with those in the *FK* model ($p < 0/05$). The mRNA levels of p16 were significantly lower in the *ASC* model compared with those in the *Allo* model ($p < 0.05$), while p16 mRNA levels in the *FK* model showed tendency to be high compared with the other models (Fig. 6b).

These results indicate that suppressing T-cell immunity is necessary to avoid rejection, but not sufficient for controlling inflammation, avoiding cellular senescence, and promoting liver regeneration. ASC therapy is thought to have the potential to modulate inflammation, but not to avoid rejection.

In order to avoid rejection and efficiently progress liver regeneration, it seems necessary to consider a combination of these treatments or to establish a new treatment strategy.

4. Discussion

In the current study, we have established HSVtk mice with normal immunity, and the liver regeneration model by transplanting of isolated hepatocytes into the HSVtk mice after GCV administration. Using this system, we investigated the process of hepatocyte engraftment and rejection after transplantation, and the sequential changes in liver histology and hepatic environment which relate to regeneration of the liver.

The combination of human TK and GCV is a system to cause death to target cell and often used for gene therapy of cancer [24,25]. GCV is selectively converted by TK to a guanosine analogue, into a monophosphorylated form which is then further phosphorylated. The generated GCV triphosphate causes chain termination by incorporation into replicating DNA as well as inhibition of DNA polymerase alpha, thereby causes apoptosis in the TK expressing cells. In addition, GCV-triphosphate is cytotoxic and causes cell death to the neighboring cells even without TK expression, and it may cause nonapoptotic cell death to those cells [26]. In the current study, we observed scattered apoptotic cells in the livers of the HSVtk mice at the early time point (0 w) after GCV administration. However, subsequent histological examination revealed that degenerated hepatocytes with enlarged cytoplasm and nuclei and inflammatory cell infiltration were the main histological findings, and apoptotic hepatocytes were rarely observed. These histological features, together with the increased mRNA levels of p16, p21, and those of inflammatory cytokines, such as TNF-α, IL-1β, IL-6, and impairment of DNA replication, suggest the cellular senescence with cell cycle arrest in the hepatocytes is the main pathological condition in the HSVtk mice treated by GCV.

It has been recognized that cellular senescence and cell cycle arrest is involved in the pathogenesis of liver failure and various chronic liver diseases [27,28]. While the study for liver regeneration to date has been mainly executed using rodent models of partial hepatectomy [29,30], ischemia/reperfusion liver injury [31], and acute liver failure caused by CCl_4, concanavalin A. etc [32,33], we believe that the novel models used in the current study are more compatible for the study of liver regeneration treatment for the persistent or late-on-set liver failure.

In the *Auto* model, despite transplantation of rather small number of PHs of 1×10^6, transplanted hepatocytes proliferated to nearly half of the hepatocytes in the liver (Fig. 3a–c). It is also notable that the resident hepatocytes recovered from the senescent condition, and the regained almost normal morphology with normal size and shape of nucleus and cytoplasm. It occurred even in the mice with low RIs.

In the *Auto* model, transient elevation of mRNA levels of inflammatory cytokines/chemokines, cell surface markers, and HGF at 1 and 2 w was characteristic compared to the other models, and its relation to the recovery of hepatocytes from senescent condition is likely. It has been reported that inflammatory cytokines and growth factors known to be induced during severe liver injury, such as TNF-α, IL-6, TGF- α, HGF, and EGF, promote survival and proliferation of hepatocytes [34,35]. Therefore, it is possible that some of these factors including TNF-α have closely related to hepatocyte recovery from cellular senescence and subsequent proliferation including transplanted PHs.

The molecules such as TNF-α, IL-1β, HGF, and some chemokines, of which mRNA expression levels were elevated at 1 and 2 w in the *Auto* model, are promoted by NFκB activation. They are identical to the group of molecules produced through activation of NFκB in senescent cells, which is called senescence-associated secretory phenotype (SASP) [36]. It is reasonable to assume that the transient increase in the mRNA expression of these molecules cannot be explained by cellular senescence alone, but is triggered by PH transplantation. There are various possibilities for this hypothesis, including the activation of the NFκB pathway by interactions between transplanted PHs and LSECs, HSCs, and Kupffer cells, or by the infiltrating inflammatory cells, such as T cells and macrophages, but they have not been elucidated in the current study.

Regarding the above hypothesis, one notable point is the transient decline in p21 mRNA levels at 1 and 2 w in the *Auto* and *Allo* models, both received PH transplantation. Regarding this phenomenon, we considered the involvement of Notch signaling pathway. While p21 is induced by its upstream molecule, p53, murine double minute 2 (Mdm2), an E3 ubiquitin ligase, is reported to cause the degradation of p53, as a major molecule involved in the suppression of p53 activity [37]. And Mdm2 is activated by Notch signaling and is reported to ubiquitinate and activate the intracellular portion of the Notch receptor [38]. It is also known that Notch signaling is involved in the activation of the NF*k*B pathway [39].

However, given that p16 also showed a downward trend at the same time, other factors may also be considered. Since we do not have direct evidence for above hypothesis, further study is necessary to confirm it.

In the current study, we also tried to find the way to rescue transplanted allogenic PHs from the rejection by recipient immune system. Since liver fibrosis was enhanced in the *Allo* model compared with the *Sham* model, it is quite important to avoid the immune rejection in cell transplantation therapy to evade from this worrying outcome.

We tested the efficacy of FK506 and ASCs for the treatment against immune rejection, and found out that only FK506 enabled the engraftment of transplanted allogenic PHs. Therefore, the use of FK506 seems reasonable for the treatment against immune rejection. But there are some concerns about this treatment, such as loss of BW in the *FK* mice which made the continuation of the treatment difficult in the current study, and the tendency of increase in hepatic p16 an p21evels which relates cellular senescence.

On the other hand, treatment with ASC did not prevent rejection, but did reduce inflammation and improved the condition of mice, including increase of BW. Furthermore, ASC administration also caused tendency to decrease the mRNA levels of p16 and p21, and possible improvement in histology. Mesenchymal stem cells including ASC are known to have regulatory effects on various inflammatory cells (probably other than $CD8^+$ T cell) [18,19], and actually exerted an anti-inflammatory effect in this model as well. Therefore, it is thought that the immunoregulatory action of ASC may have suppressed the senescence of hepatocytes in this model. The usefulness of ASC administration itself for the treatment of liver failure should also be investigated.

However, we have to note that the administration protocols of FK506 and ASCs used in the current study are still preliminary. It is necessary to examine appropriate timing, number of times and intervals of administrations for both FK506 and ASCs.

There are several limitations and remained questions in the current study besides described above. Since the difference in the background of mice alter the sensitivity to GCV, comparison in hepatic histology and mRNA expressions between the *Sham* and *Allo* model should be more deliberately. We tried to adjust the ALT levels before transplantation in all the models, but we should have added the appropriate control for the *Allo* model, such as HSVtk/Balb with GCV treatment. We did not have method to predict RI after hepatocyte transplantation, and had to sacrifice mice at each time point. If we have surrogate marker for RI, it may make the sequential analysis easier and long-term analysis possible. We may have to think about more extended method for gene expression analysis, such as RNA sequence and single-cell analysis, since there are many other genes of interest other than we analyzed in the current study, and the cells that constitute the liver are diverse. All of these should be considered in the further study.

In conclusion, the current HSVtk/GCV system was confirmed to be useful for studying the mechanism of liver regeneration and immune rejection responses in the hepatocyte and hepatocyte-like cell transplantation treatment, and for studying the effective treatment methods to avoid immune rejection.

Declaration of competing interest

The authors declare that they have no known competing financial interests or personal relationships that could have appeared to influence the work reported in this paper.

Acknowledgement

The authors thank Ms. Machi Yamamoto, Kanako Yamazaki, Ai Imaida, Junko Hori, Mr. Ayumu Kanbe for technical assistance. This research is partially supported by Japan Society for the Promotion of Science (JSPS) KAKENHI Grant Number JP16K09354, JP21K07959, the program on the Innovative Development and the Application of New Drugs for Hepatitis B from Japan Agency for Medical Research and Development (AMED), #20fk0310106h0004, #21fk0310106s0605, #22fk0310516s0201.

Appendix A. Supplementary data

Supplementary data to this article can be found online at https://doi.org/10.1016/j.bbrep.2022.101382.

References

[1] J. Neuberger, An update on liver transplantation: a critical review, J. Autoimmun. 66 (2016) 51–59.
[2] A. Soyama, S. Eguchi, H. Egawa, Liver transplantation in Japan, Liver Transplant. 22 (2016) 1401–1407.
[3] B.E. Tasdogan, S. Akosman, M. Gurakar, C. Simsek, A. Gurakar, Update on liver transplantation: what is new recently? Euroasian J. Hepato-Gastroenterol. 9 (2019) 34–39, https://doi.org/10.5005/jp-journals-10018-1293.
[4] S.B. Brown, Pros and cons of living donor liver transplant, Gastroenterol. Hepatol. 4 (2008) 622–624.
[5] J.N. Itri, M.T. Heller, M.E. Tublin, Hepatic transplantation: postoperative complications, Abdom. Imag. 38 (2013) 1300–1333.
[6] M.M. López, J.E. Valenzuela, F.C. Alvarez, M.R. López-Alvarez, C.S. Cecilia, P. P. Paricio, Long-term problems related to immunosuppression, Transpl. Immunol. 17 (2006) 31–35.
[7] V. Iansante, R.R. Mitry, C. Filippi, E. Fitzpatrick, A. Dhawan, Human hepatocyte transplantation for liver disease: current status and future perspectives, Pediatr. Res. 83 (2018) 232–240, https://doi.org/10.1038/pr.2017.284.
[8] L.Y. Lghanem, I.M. Mansour, N. Abulata, M.M. Akl, Z.A. Demerdash, H.G. El Baz, S. S. Mahmoud, S.H. Mohamed, F.S. Mahmoud, A.S.M. Hassan, Liver macrophage depletion ameliorates the effect of mesenchymal stem cell transplantation in a murine model of injured liver, Sci. Rep. 9 (2019) 35, https://doi.org/10.1038/s41598-018-37184-4.
[9] T. Katsuda, J. Matsuzaki, T. Yamaguchi, Y. Yamada, M. Prieto-Vila, K. Hosaka, A. Takeuchi, Y. Saito, T. Ochiya, Generation of human hepatic progenitor cells with regenerative and metabolic capacities from primary hepatocytes, Elife 8 (2019), e47313, https://doi.org/10.7554/eLife.47313.
[10] K. Takayama, N. Akita, N. Mimura, R. Akahira, Y. Taniguchi, M. Ikeda, F. Sakurai, O. Ohara, T. Morio, K. Sekiguchi, H. Mizuguchi, Generation of safe and therapeutically effective human induced pluripotent stem cell-derived hepatocyte-like cells for regenerative medicine, Hepatol. Commun. 1 (2017) 1058–1069.
[11] H.A. Reza, R. Okabe, T. Takebe, Organoid transplant approaches for the liver, Transpl. Int. 34 (2021) 2031–2045, https://doi.org/10.1111/tri.14128.
[12] M. Hasegawa, K. Kawai, T. Mitsui, K. Taniguchi, M. Monnai, M. Wakui, M. Ito, M. Suematsu, G. Peltz, M. Nakamura, H. Suemizu, The reconstituted "humanized liver" in TK-NOG mice is mature and functional, Biochem. Biophys. Res. Commun. 405 (2011) 405–410.
[13] H. Yamazaki, H. Suemizu, M. Shimizu, S. Igaya, N. Shibata, M. Nakamura, G. Chowdhury, F.P. Guengerich, In vivo formation of dihydroxylated and glutathione conjugate metabolites derived from thalidomide and 5-hydroxythalidomide in humanized TK-NOG mice, Chem. Res. Toxicol. 25 (2012) 274–276.
[14] K. Kosaka, N. Hiraga, M. Imamura, S. Yoshimi, E. Murakami, T. Nakahara, Y. Honda, A. Ono, K. Kawaoka, M. Tsuge, H. Abe, C.N. Hayes, D. Miki, H. Aikata, H. Ochi, Y. Ishida, C. Tateno, K. Yoshizato, T. Sasaki, K. Chayama, A novel TK-NOG based humanized mouse model for the study of HBV and HCV infections, Biochem. Biophys. Res. Commun. 441 (2013) 230–235.
[15] J.J. Fung, S. Todo, A. Jain, J. Mccauley, M. Alessiani, C. Scotti, T.E. Starzl, Conversion from cyclosporine to FK506 in liver allograft recipients with cyclosporine-related complications, Transplant. Proc. 22 (1990) 6–12.
[16] Z. Yu, X. Zhou, S. Yu, H. Xie, S. Zheng, IL-15 is decreased upon CsA and FK506 treatment of acute rejection following heart transplantation in mice, Mol. Med. Rep. 11 (2015) 37–42.
[17] K. Shao, Y. Lu, J. Wang, X. Chen, Z. Zhang, X. Wang, X. Wang, H. Yang, G. Liu, Different effects of tacrolimus on innate and adaptive immune cells in the allograft transplantation, Scand. J. Immunol. 83 (2016) 119–127.
[18] R. Nagaya, M. Mizuno-Kamiya, E. Takayama, H. Kawaki, I. Onoe, T. Tanabe, K. Nagahara, N. Kondoh, Mechanisms of the immunosuppressive effects of mouse adipose tissue-derived mesenchymal stromal cells on mouse alloreactivity stimulated spleen cells, Exp. Ther. Med. 7 (2013) 17–22.
[19] D.K. Lee, S.U. Song, Immunomodulatory mechanisms of mesenchymal stem cells and their therapeutic applications, Cell. Immunol. 326 (2018) 68–76.
[20] M. Shi, Z. Liu, Y. Wang, R. Xu, Y. Sun, M. Zhang, X. Yu, H. Wang, L. Meng, H. Su, L. Jin, F.S. Wang, A pilot study of mesenchymal stem cell therapy for acute liver allograft rejection, Stem Cells Transl. Med. 6 (2017) 2053–2061.
[21] Y. Kanda, Investigation of the freely available easy-to-use software 'EZR' for medical statistics, Bone Marrow Transplant. 48 (2013) 452–458, https://doi.org/10.1038/bmt.2012.244.
[22] L.D. DeLeve, Liver sinusoidal endothelial cells and liver regeneration, J. Clin. Invest. 123 (2013) 1861–1866, https://doi.org/10.1172/JCI66025.
[23] E. Hara, ParrybRD. Smith, H. Tahara, S. Stone, G. Peters, Regulation of $p16C^{DKN2}$ expression and its implications for cell immortalization and senescence, Mol. Cell Biol. 16 (1996) 859–867, https://doi.org/10.1128/MCB.16.3.859.
[24] M. Mesnil, H. Yamasaki, Bystander effect in herpes simplex virus-thymidine kinase/ganciclovir cancer gene therapy: role of gap-junctional intercellular communication, Cancer Res. 60 (2000) 3989–3999.
[25] A. Al-Hendy, A.M. Magliocco, T. Al-Tweigeri, G. Braileanu, N. Crellin, H. Li, T. Strong, D. Curiel, P.J. Chedrese, Ovarian cancer gene therapy: repeated treatment with thymidine kinase in an adenovirus vector and ganciclovir improves

survival in a novel immunocompetent murine model, Am. J. Obstet. Gynecol. 182 (2000) 553–559, https://doi.org/10.1067/mob.2000.104837.
[26] D. Srivastava, G. Joshi, K. Somasundaram, R. Mulherkar, Mode of cell death associated with adenovirus-mediated suicide gene therapy in HNSCC tumor model, Anticancer Res. 31 (2011) 3851–3857.
[27] A. Mitselou, D. Karapiperides, I. Nesseris, T. Vougiouklakis, N.J. Agnantis, Altered expression of cell cycle and apoptotic proteins in human liver pathologies, Anticancer Res. 30 (2010) 4493–4501.
[28] N. Huda, G. Liu, H. Hong, S. Yan, B. Khambu, X.M. Yin, Hepatic senescence, the good and the bad, World J. Gastroenterol. 25 (2019) 5069–5081, https://doi.org/10.3748/wjg.v25.i34.5069.
[29] S. Togo, H. Makino, T. Kobayashi, M. Morita, T. Shimizu, T. Kubota, Y. Ichikawa, T. Ishikawa, Y. Okazaki, Y. Hayashizaki, H. Shimada, Mechanism of liver regeneration after partial hepatectomy using mouse cDNA microarray, J. Hepatol. 40 (2004) 464–471, https://doi.org/10.1016/j.jhep.2003.11.005.
[30] T. Itoh, A. Miyajima, Liver regeneration by stem/progenitor cells, Hepatology 59 (2014) 1617–1626, https://doi.org/10.1002/hep.26753. Epub 2014 Feb 14.
[31] T. Konishi, A.B. Lentsch, Hepatic ischemia/reperfusion: mechanisms of tissue injury, repair, and regeneration, Gene Expr. 17 (2017) 277–287, https://doi.org/10.3727/105221617X15042750874156.
[32] Z. Meng, Y. Wang, L. Wang, W. Jin, N. Liu, H. Pan, L. Liu, L. Wagman, B. M. Forman, W. Huang, FXR regulates liver repair after CCl_4-induced toxic injury, Mol. Endocrinol. 24 (2010) 886–897, https://doi.org/10.1210/me.2009-0286.
[33] A.B. Ya'acov, H. Meir, L. Zolotaryova, Y. Ilan, E. Shteyer, Impaired liver regeneration is associated with reduced cyclin B1 in natural killer T cell-deficient mice, BMC Gastroenterol. 17 (2017) 44, https://doi.org/10.1186/s12876-017-0600-2.
[34] T.A. Zimmers, I.H. McKillop, R.H. Pierce, J.Y. Yoo, L.G. Koniaris, Massive liver growth in mice induced by systemic interleukin 6 administration, Hepatology 38 (2003) 326–334.
[35] F. Böhm, U.A. Köhler, T. Speicher, S. Werner, Regulation of liver regeneration by growth factors and cytokines, EMBO Mol. Med. 2 (2010) 294–305, https://doi.org/10.1002/emmm.201000085.
[36] R. Salama, M. Sadaie, M. Hoare, M. Narita, Cellular senescence and its effector programs, Genes Dev. 28 (2014) 99–114, https://doi.org/10.1101/gad.235184.113.
[37] K. Vermeulen, Z.N. Berneman, D.R. Van Bockstaele, Cell cycle and apoptosis, Cell Prolif 36 (2003) 165–175, https://doi.org/10.1046/j.1365-2184.2003.00267.x.
[38] D. Dutta, V. Sharma, M. Mutsuddi, A. Mukherjee, Regulation of Notch signaling by E3 ubiquitin ligases, FEBS J. 289 (2022) 937–954, https://doi.org/10.1111/febs.15792.
[39] F. Ayaz, B.A. Osborne, Non-canonical notch signaling in cancer and immunity, Front. Oncol. 4 (2014) 345, https://doi.org/10.3389/fonc.2014.00345.